MIT Libraries | DSpace@MIT

MIT Open Access Articles

Methanogenic burst in the end-Permian carbon cycle

Massachusetts Institute of Technology

Methanogenic burst in the end-Permian carbon cycle

Daniel H. Rothman[a,b,1], Gregory P. Fournier[c], Katherine L. French[b], Eric J. Alm[c], Edward A. Boyle[b], Changqun Cao[d], and Roger E. Summons[b]

[a]Lorenz Center, [b]Department of Earth, Atmospheric, and Planetary Sciences, and [c]Department of Biological Engineering, Massachusetts Institute of Technology, Cambridge, MA 02139; and [d]State Key Laboratory of Palaeobiology and Stratigraphy, Nanjing Institute of Geology and Palaeontology, Chinese Academy of Sciences, Nanjing 210008, China

The end-Permian extinction is associated with a mysterious disruption to Earth's carbon cycle. Here we identify causal mechanisms via three observations. First, we show that geochemical signals indicate superexponential growth of the marine inorganic carbon reservoir, coincident with the extinction and consistent with the expansion of a new microbial metabolic pathway. Second, we show that the efficient acetoclastic pathway in *Methanosarcina* emerged at a time statistically indistinguishable from the extinction. Finally, we show that nickel concentrations in South China sediments increased sharply at the extinction, probably as a consequence of massive Siberian volcanism, enabling a methanogenic expansion by removal of nickel limitation. Collectively, these results are consistent with the instigation of Earth's greatest mass extinction by a specific microbial innovation.

methanogenesis | horizontal gene transfer | microbial evolution | biogeochemical dynamics

The greatest rate of taxonomic loss during the end-Permian extinction—the most severe in the fossil record (1)—occurs within 20,000 y, beginning about 252.28 million years ago (Ma) (2) at a time precisely coincident (2) with geochemical signals indicating a severe and equally rapid perturbation to Earth's carbon cycle (1–6). Although probably related, neither the cause of the extinction nor the origin of the change in the carbon cycle is known. One possible linkage derives from the observation that massive Siberian volcanism occurs at roughly the same time as the extinction (7, 8). However, quantitative estimates of direct volcanic outgassing are much too small to account for the changes in the carbon cycle (9). Secondary effects of Siberian volcanism, such as the combustion of huge deposits of coal (10) or other forms of organic carbon (11), are more attractive quantitatively but still difficult to reconcile with observed geochemical changes (1–6). Reports of marine anoxia in the Late Permian (5, 12, 13) also indicate changes in the carbon cycle. Moreover, the notion that a disturbance of the carbon cycle plays a significant role as a "kill mechanism" derives considerable support from observations of physiological differences between species that survived the extinction and those that did not (14–16).

Here we relate the principal observations of end-Permian environmental change—massive volcanism and changes in marine CO_2 and O_2 levels—to the transfer of genetic material, from a cellulolytic bacterium to a methanogenic archaeon, that enabled efficient methanogenic degradation of organic carbon (17). Our analysis is constructed from three key observations. First, we show that the form of time-dependent changes in the carbon isotopic record indicates an instability within the carbon cycle that is inconsistent with volcanic combustion of organic sediments but consistent with the expansion of a new microbial metabolic pathway. Second, we identify this pathway with efficient acetoclastic methanogenesis and show that the age of the last common ancestor of *Methanosarcina*, the genus using this pathway, is consistent with the time of the extinction. Because methanogens are limited by nickel (18, 19), the third component of our study presents an analysis of nickel deposited in South China sediments. We find that nickel concentrations rose just before the extinction, presumably as a consequence of Siberian volcanism, providing a mechanism not only to enhance the methanogenic expansion

and its perturbation to the carbon cycle but also to amplify the development of marine anoxia. Taken as a whole, these results reconcile an array of apparently disparate observations about the end-Permian event.

Growth of the Marine Carbon Reservoir

Fig. 1*A* displays the carbon-isotopic record in Meishan, China (5). Immediately preceding the extinction event, the isotopic composition δ_1 of carbonate carbon declines by about 7‰ during a period of about 100 thousand years (Kyr), first slowly, and subsequently rapidly. At the same time, the isotopic composition δ_2 of organic carbon also changes. We seek the physical fluxes in the carbon cycle that predict the chemical signals $\delta_1(t)$ and $\delta_2(t)$. Of particular interest is whether the apparent downward acceleration of the carbonate signal can provide a quantitative indication of the underlying biogeochemical dynamics.

To obtain such understanding, we consider the carbon cycle to be a simple exchange between globally mixed reservoirs of inorganic and organic carbon, via photosynthesis and respiration (20), and assume that the isotopic changes represent a perturbation from a preexisting steady state. We assume that the system is perturbed by an influx of isotopically light inorganic carbon of constant isotopic composition $\delta_i' < \delta_1$, forcing δ_1 to decline out of its steady state. Because organic carbon is isotopically light, a decrease in its rate of burial is effectively indistinguishable from such light inputs. However, changes in organic burial can account for only a negligible fraction of the peak perturbed flux (*SI Text*). Changes in the burial flux of carbonate carbon are limited to an even smaller impact because its isotopic composition is identical to that of the inorganic reservoir. We therefore hold both burial

Significance

The end-Permian extinction is the most severe biotic crisis in the fossil record. Its occurrence has been attributed to increased CO_2 levels deriving from massive Siberian volcanism. However, such arguments have been difficult to justify quantitatively. We propose that the disruption of the carbon cycle resulted from the emergence of a new microbial metabolic pathway that enabled efficient conversion of marine organic carbon to methane. The methanogenic expansion was catalyzed by nickel associated with the volcanic event. We support this hypothesis with an analysis of carbon isotopic changes leading up to the extinction, phylogenetic analysis of methanogenic archaea, and measurements of nickel concentrations in South China sediments. Our results highlight the sensitivity of the Earth system to microbial evolution.

Fig. 1. Carbon isotopic signals immediately preceding the end-Permian extinction in Meishan, China, indicate superexponential growth of the marine inorganic carbon reservoir. (*A*) Inorganic (δ_1, blue) and organic (δ_2, green) carbon isotopic changes (5). The dates at both ends of the time axis are resolved within ± 0.08 Myr (2); in between, time is interpolated linearly in proportion to stratigraphic height. The peak extinction activity occurs at approximately -252.28 Myr (2). (*B*) Reconstruction (solid blue line) of the dimensionless mass $M(t)$ added to the marine inorganic carbon reservoir, assuming initial condition $M = 0$ and an influx of isotopically light carbon with isotopic composition $\delta_i' = -28‰$. (*Inset*) The same curve plotted on log-linear axes; the concave upward curvature suggests that $M(t)$ grows super-exponentially. The dashed red line compares $M(t)$ to a superexponential growth law proportional to $(t_c - t)^{-1}$, where the critical time t_c is coincident with the extinction peak.

rates constant to maintain simplicity. The mass $m_1(t)$ of the inorganic reservoir then grows with time t in response to the increased inputs, by an amount $m_1'(t) = m_1 - m_1^*$, where m_1^* is the initial, steady-state, size of the reservoir. The normalized perturbation $M = m_1'/m_1^*$ is then straightforwardly related to changes in the geochemical signals by (*SI Text*)

$$h\frac{dM}{dt} = \frac{d\delta_1}{dt}M + F\left(\delta_1, \delta_2, \frac{d\delta_1}{dt}\right), \qquad [1]$$

where $h = \delta_i' - \delta_1(t) < 0$ determines the scale of the perturbation and the "force" F is a weighted sum of two nonsteady-state effects: the nonzero derivative $d\delta_1/dt$ and the departures of δ_1 and δ_2 from their unperturbed values. The solution of Eq. **1** for $M(t)$ provides the normalized time-dependent perturbation of the marine reservoir of dissolved inorganic carbon (DIC). The way in which the DIC reservoir grows with time is a function of how it is forced out of its steady state; consequently, knowledge of $M(t)$ can be used to test models of the end-Permian carbon cycle.

The form of Eq. **1** provides an immediate clue. Because $\delta_1(t)$ accelerates sharply downward, $d\delta_1/dt$ is increasingly negative. Consideration of the unforced ($F = 0$) equation then suggests that M grows exponentially or faster. Numerical solutions of Eq. **1** confirm this view. Fig. 1*B* plots $M(t)$ for the case $\delta_i' = -28‰$, representative of the isotopic composition of remineralized

organic carbon, assuming a constant sediment accumulation rate between the known dates (2). The curvature of the log-linear plot in Fig. 1*B*, *Inset* suggests that the growth of $M(t)$ is faster than exponential. (Although the total quantity of light carbon required for the isotopic excursion depends on δ_i' (1, 2, 6, 9), the shape of $M(t)$ is independent of δ_i' when, as here, δ_i' is much smaller than δ_1.) Superexponential growth of the marine inorganic carbon reservoir implies that the carbon cycle behaves nonlinearly. As we show later, a simple dynamical mechanism containing a leading-order nonlinearity predicts superexponential growth proportional to $(t_c - t)^{-1}$. Such a growth law, where t_c is coincident with the extinction peak, is given by the red-dashed line in Fig. 1*B*. The burst near t_c—an incipient singular blow-up—can be traced back to the rapid downward acceleration of the carbonate signal, a feature that is not exhibited by the linearly decreasing isotopic excursions of the Early Triassic (21).

Fig. 2 combines this analysis with the analogous carbon isotopic signal in the Gartnerkofel-I core drilled in the Carnic Alps, Austria (3, 4). Cyclostratigraphic analysis of the Gartnerkofel core indicates that the sediment accumulation rate over the corresponding interval is approximately constant (22). When the accumulation rate is set to 22.5 cm/Kyr, approximately within a factor of 2 of the earlier estimate (22), reconstructions of $M(t)$ for Gartnerkofel are qualitatively similar to that for Meishan. Fig. 2, which superposes both reconstructions in linear, log-linear, and log–log plots, confirms the inferences already drawn from the Meishan data. Moreover, the similarity of the Meishan and Gartnerkofel reconstructions validates our assumption of a constant accumulation rate at Meishan. We conclude that $M(t)$ grows no slower than exponentially, and likely superexponentially.

These observations impose constraints on interpretations of end-Permian environmental change. For example, CO_2 released to the atmosphere from a single, massive Siberian coal–basalt eruption (10) would be mostly transferred to the oceans after about 10^2–10^3 y (23). The uptake rate would decrease with time as the oceans acidify, reducing their capacity to take up more CO_2 (23). $M(t)$ would then grow sublinearly, qualitatively different from what is shown in Figs. 1 and 2. Alternatively, such an eruption could be more gradual, limited by the rate at which vents form to release overpressured gas arising from contact metamorphism in intruded sills (11). The pressure released by each vent decreases overpressurization. Wherever the pressure is lowered, the rate of vent formation would decrease, and $M(t)$ would again be sublinear. It is possible, however, that vents were sufficiently dispersed in space so that their formation times were essentially independent and randomly distributed over some (possibly small) interval of time; in this case, one expects a roughly constant rate of CO_2 emission, and $M(t)$ would grow linearly. Likewise, the release of methane from methane hydrates (1, 9) could be clustered in time, but there is no reason to expect total methane emissions to grow much faster than linearly, in part because any resulting warming—a potential positive feedback— would be only logarithmically sensitive to increased CH_4 and CO_2 levels (24). Each of these scenarios would produce geochemical signals that qualitatively differ from those predicted by exponential or superexponential growth (*SI Text*). The constraints provided by this reasoning derive only from the shape of $M(t)$, not the quantity of isotopically light carbon required for the event.

The Carbon Source and Its Remobilization
We seek a mechanism that can result in growth of $M(t)$ that is exponential or faster. Because such an upheaval of the carbon cycle implies substantial changes within the microbial biosphere, we hypothesize that the perturbation arises from the emergence of a new regime of microbial metabolic activity. We show below how such a mechanism leads to the observed dynamics. Before doing so, we first identify two important ingredients of our hypothesis: a suitably large source of degradable organic carbon
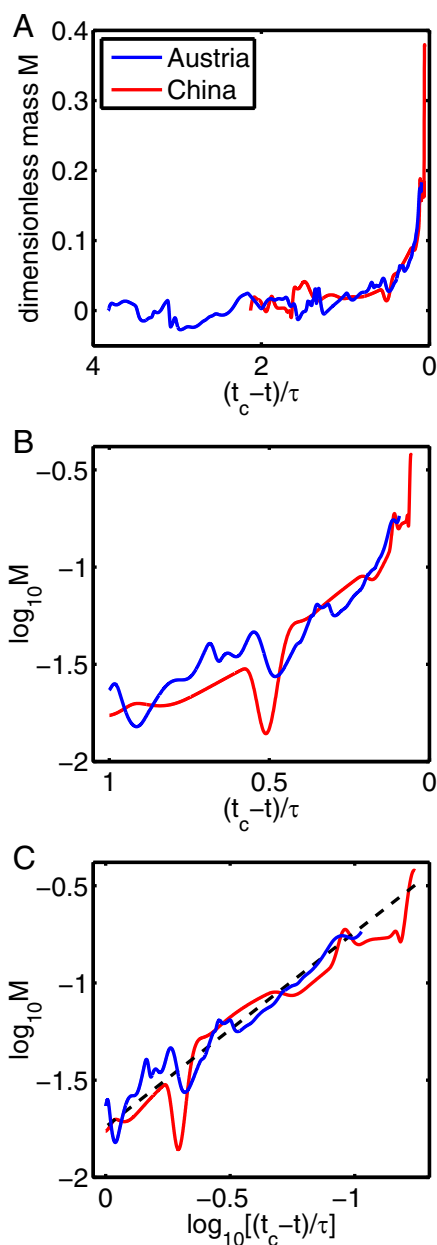
Fig. 2. Rescaled reconstructions of the mass $M(t)$ of the marine inorganic carbon reservoir for both the Meishan (red) and Gartnerkofel (blue) data, as a function of rescaled time $(t_c - t)/\tau$, where $\tau = 100$ Kyr and time advances to the right. (*A*) Plots of M vs. $(t_c - t)/\tau$ show that both curves behave similarly with respect to a critical time t_c. (*B*) Plots of $M(t)$ on log-linear axes suggest that both curves grow superexponentially. (*C*) Plots of $M(t)$ on log–log axes compare well to a straight line (dashed black) with slope -1, suggesting that both reconstructions grow like $(t_c - t)^{-1}$.

and the new metabolic pathway that would be favored for its consumption.

In terms of the modern carbon cycle (25), our reconstructions of $M(t)$ require about 7,000–14,000 Gt of remineralizable organic carbon. In the Late Permian, a low-O_2 marine environment (5, 12, 13) would have increased the concentration of organic matter in sediments. The high values of δ_1 immediately before the perturbation suggest that organic carbon was sequestered in sediments at a rate at least 50% greater than usual (*SI Text*), which, in modern terms (25), corresponds to excess sequestration of at least 0.08 Gt C yr^{-1}. Integrated over the first 175 Kyr of

Fig. 1*A*, this corresponds to 14,000 Gt C. We suggest that a substantial fraction remained remineralizable and relatively labile compared with organic carbon in modern sediments, thereby overcoming the apparent limitations (2) posed by the relatively small size of modern pools of isotopically light organic carbon (26) (e.g., methane hydrates, fossil fuels, soil organic carbon, and peat).

The accumulation of sedimentary organic matter would have been especially sensitive to changes in the biosphere's ability to metabolize the products of fermentation. Among these products, acetate provides a major growth substrate for methanogens. The conversion of acetate to methane by methanogenic archaea—acetoclastic methanogenesis (27)—begins by activating acetate to acetyl coenzyme A (acetyl-CoA). Carbon monoxide dehydrogenase (CODH) then catalyzes the cleavage of acetyl-CoA, after which, in common with the utilization of all methanogenic substrates, methyl-coenzyme M reductase (MCR) catalyzes the reduction of a methyl group to methane (27). The activation to acetyl-CoA within methanogens occurs via two different pathways in two distinct groups of organisms: Members of the family *Methanosaetaceae* use a single-step acetyl-CoA synthase (ACS) pathway, whereas some members of the genus *Methanosarcina* use a two-step acetate kinase (AckA)-phosphoacetyl transferase (Pta) pathway (27). The AckA/Pta pathway is more energy efficient, requiring only one ATP molecule per acetate molecule activated, whereas the ACS pathway requires two (28). Growth on acetate using the low-efficiency ACS pathway within *Methanosaeta* is thermodynamically possible because of unique, poorly understood innovations in their electron transport chain (29); this limitation may be responsible for their observed slow rate of growth (30).

Fournier and Gogarten (17) have recently shown that the high-efficiency pathway in *Methanosarcina* evolved via a single horizontal gene transfer event, probably from a clade of cellulolytic bacteria belonging to the class *Clostridia*, after the mid-Ordovician evolution of vascular land plants (450–500 Ma). This is the only methanogenic pathway shown to have evolved via gene transfer. It also appears to be a conspicuously recent event within the evolution of methanogenesis, as all other methanogenic pathways have a broader phylogenetic distribution implying much more ancient origins. *Methanosaeta* may be more widespread in modern low-acetate marine environments (31). However, the dominance of the high-efficiency AckA-Pta pathway at high acetate concentrations (32) combined with the greater growth potential of *Methanosarcina* suggests that conditions for the emergence of acetoclastic *Methanosarcina*—specifically, a low-O_2 marine environment (5, 12, 13) and the accumulation of sedimentary organic matter—would have been favorable in the Late Permian. Moreover, reports of significantly reduced marine sulfate concentrations (33–36) suggest that competition from sulfate-reducing bacteria would have been diminished, thereby amplifying the importance of methanogenesis in Late Permian marine sediments.

Phylogenetic Analysis

The relevance of acetoclastic *Methanosarcina* to the end-Permian event depends crucially on the timing for the ancestor of this group. To obtain an estimate for this date, we reconstructed archaeal phylogenies from 50 representative genomes and constructed relaxed molecular clock chronograms using PhyloBayes 2.3 (*SI Text*). Fig. 3*A* illustrates our results. To estimate the time τ_m of the last common ancestor of known acetoclastic representatives of *Methanosarcina*, we generated chronograms using four independent ribosome-based datasets, separately containing 29 concatenated universally conserved ribosomal proteins, 12 concatenated archaeal-specific ribosomal proteins, 16S ribosomal RNA, and 23S ribosomal RNA. The phylogeny of these ribosomal components reflects the vertical cellular history of the
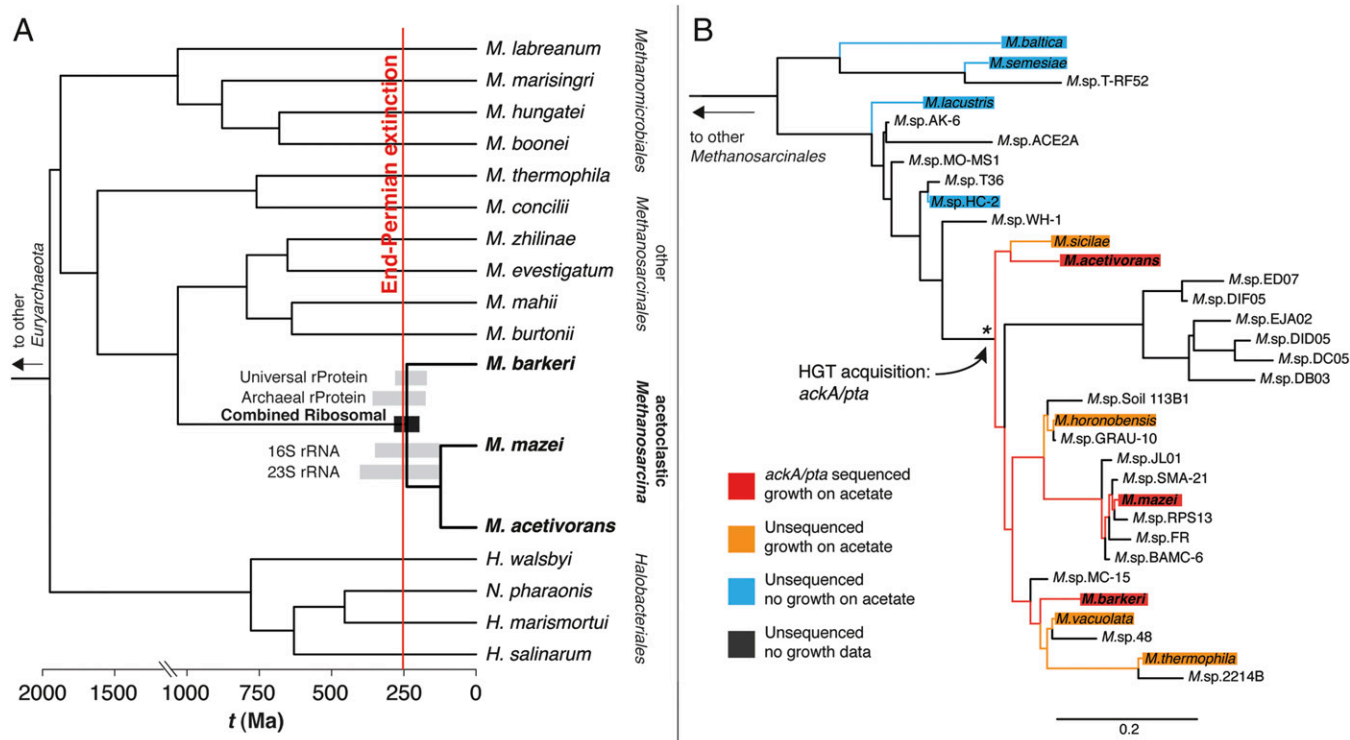
Fig. 3. (*A*) Subtree of calibrated archaeal chronogram showing *Methanosarcinales* and related groups. Acetoclastic *Methanosarcina* (bold) groups with other members of *Methanosarcinales*, including the distantly related acetoclastic *Methanosaetaceae* (*M. thermophila, M. concilii*). Shaded bars indicate the estimated acetoclastic *Methanosarcina* ancestor age ranges (±1 SD) for each dataset. The combined estimate of 240±41 Myr is indicated by the black bar. The tree was generated from the Universal rProtein dataset, with the age of acetoclastic *Methanosarcina* adjusted to match the combined estimate. (*B*) Members of the genus *Methanosarcina* shown to grow on acetate all descend from the ancestor of sequenced clade representatives containing the transferred *ackA/pta* genes (*). congruent with the age-estimated node in *A*. The relationships between known taxa are represented by their 16S phylogenetic tree.

Methanosarcinales, including *Methanosarcina* and its descendants, the recipient lineage of the *ackA/pta* transfer. We further assume that ribosomal sequences evolve in a relatively clock-like manner, providing more reliable dates than most other genes in the absence of internal calibration. Our four independent age estimates, shown by the gray bars in Fig. 3*A*, are consistent with each other. Combining them together yields the joint estimate $\tau_m = 240 \pm 41$ Ma depicted by the black bar in Fig. 3*A*, strikingly close to the end-Permian extinction (*SI Text*). The discrepancy with a previous estimate (37) derives from the earlier use of an autocorrelated clock model that is less reliable for the estimation of deep-time phylogenies than the approach used here (*SI Text*).

Additional phylogenetic character analysis of 16S sequences from 33 species within the genus *Methanosarcina* lends increased precision to the placement of the gene transfer event within the chronogram of Fig. 3*A*. As shown in Fig. 3*B*, all *Methanosarcina* strains that grow readily on acetate diverge within the *M. acetivorans/M. mazei/M. barkeri* clade, whereas all strains shown not to grow on acetate diverge more deeply within the tree. This result supports a relatively recent horizontal transfer of *ackA/pta* within the *Methanosarcina* genus (*SI Text*), at a time consistent with the Late Permian. The combined results of Fig. 3 therefore support the hypothesis that the emergence of the acetoclastic pathway in *Methanosarcina* provided the microbial instigation of the end-Permian burst in the carbon cycle.

Methanogenic Expansion

Wherever sulfate was limiting—because of a widespread drawdown of sulfate levels (33–36), a localized depletion by sulfate reducers, or both—the introduction of the high-efficiency acetoclastic pathway would have diminished a thermodynamic barrier (38) to greater acetate production by fermenters. Not only would acetate be converted more quickly to methane, but also sedimentary organic matter would be fermented more rapidly to acetate. *Methanosaeta* would have played a supporting role, but a preexisting steady state excludes the possibility that *Methanosaeta* itself would have excited the perturbation.

The resulting methane burst would have been oxidized to CO_2, either by anaerobic methanotrophs at the expense of any remaining sulfate or aerobically. O_2 levels, which were likely already low (5, 12, 13), would have been depressed further. Given the assumptions of an effectively unlimited substrate and a preexisting steady state, the size of the acetoclastic methanogenic niche—i.e., the carrying capacity K—would therefore have increased, at a rate proportional to the rate at which nearby sulfate and O_2 were depleted. Taking the depletion rate proportional to the methane flux, we then have $dK/dt = k_1 dA/dt$, where $A \propto M$ is the total methane production and k_1 is a conversion constant. Integrating both rates yields

$$K(t) = k_0 + k_1 A(t), \qquad [2]$$

where k_0 is the initial (unperturbed) carrying capacity. At the time scale of the geochemical signals ($>10^3$ y), the methanogenic population is always at carrying capacity. The methane production rate is therefore

$$dA/dt = \beta K, \qquad [3]$$

where β is the individual metabolic rate. Eqs. **2** and **3** describe unstable growth: Increasing methane production (A) increases

the carrying capacity (K), which in turn increases the methane production rate dA/dt. Then if β is constant, $A(t)$ grows exponentially.

However, several mechanisms may have acted to increase β. These include the aforementioned interactions with other microbial communities; warming due to higher CO_2 and methane levels; adaptive radiation (39) as subtaxa evolved to more efficiently use acetate in particular environments; and greater access to any limiting mineral nutrients as the anoxic, methanogenic niche rose upwards. Each of these mechanisms implies a functional dependence on the total methane production A. We hypothesize a linear response:

$$\beta(t) = \beta_0 + \beta_1 A(t), \qquad [4]$$

where β_0 is the initial metabolic rate and β_1 is a constant. Inserting Eqs. **2** and **4** into Eq. **3**, we obtain

$$dA/dt = a_0 + a_1 A + a_2 A^2, \qquad [5]$$

where $a_0 = \beta_0 k_0$, $a_1 = \beta_1 k_0 + \beta_0 k_1$, and $a_2 = \beta_1 k_1$. For nonzero a_2, the solution $A(t)$ blows up at a time t_c determined by initial conditions. Near t_c, the dynamics are dominated by the nonlinearity. To leading order,

$$A(t) = \frac{1}{a_2(t_c - t)}, \qquad t \to t_c, \qquad [6]$$

which is drawn as the dashed red curve in Fig. 1*B* and the dashed straight line in Fig. 2*C* (as $M \propto A$, using the best-fitting scale factor). The good fit supports the nonlinear model (Eq. **5**), but it raises an important question: As t approached t_c—the time of peak extinction activity—how could the growth of the methanogenic community have been sustained?

Nickel Limitation and the Meishan Nickel Record

Methanogens require nickel (18). The active site of the enzyme MCR, used by all methanogens, is the nickel cofactor F_{430}; moreover, the CODH enzyme complex used by acetoclastic methanogens also contains a nickel cofactor (40). Seawater concentrations of nickel have likely been beneath the limiting threshold for methanogens for roughly the last 2 billion years (19). Accordingly, we suggest that methanogenesis in Late Permian sediments was limited by nickel. If so, the methanogenic expansion would have required increased access to nickel.

Kaiho et al. (41) have reported a sharp increase in the concentration of nickel in Meishan sediments coincident with the carbon isotopic spike. Because their analysis extends only through the last 5‰ of the 7‰ carbon isotopic spike and does not consider the effects of lithologic changes, we have performed new measurements of nickel concentrations at Meishan, not only over the entire interval shown in Fig. 1 but also well above it, and have corrected our measurements for variable concentrations of carbonate (*SI Text*). Fig. 4 displays our results. Nickel concentrations before the carbon isotopic spike are typically at least twice as high as after, and are up to seven times greater just before the abrupt downturn. With such elevated concentrations, nickel would no longer limit methanogenic activity. All methanogens would have prospered, but the successful evolution and rapid expansion of acetoclastic *Methanosarcina* would have been especially favored in the substrate-rich end-Permian environment.

The nickel likely originated from Siberia. Earth's largest economic concentration of nickel is in the Noril'sk region, deposited during the emplacement of the Siberian traps (42). The Meishan nickel signal may therefore represent changes in ocean chemistry induced by the Siberian eruptions, thereby linking the growth
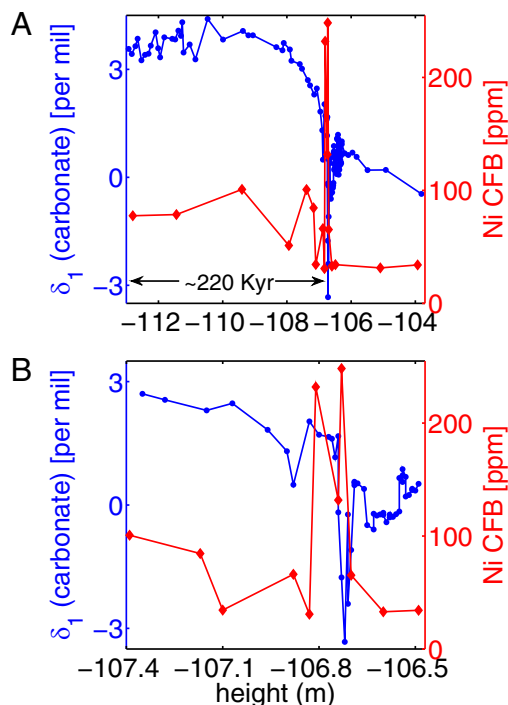

Fig. 4. Nickel concentrations (red) in the Meishan sediments, compared with the isotopic composition δ_1 of carbonate carbon (blue). (*A*) Approximately 9 m of sedimentary section. (*B*) Close-up of the changes, over a range of less than 1 m. The largest nickel concentration precedes the smallest value of δ_1. Nickel concentrations are reported in terms of a carbonate-free basis (*SI Text*).

of acetoclastic *Methanosarcina* to massive Siberian volcanism. The apparent insensitivity of nickel to redox processes (43–45) supports this interpretation. However, elemental redistribution during diagenetic redox cycling could represent an alternative cause of nickel enrichment in the sediment (46); further analysis of redox-sensitive elements will help evaluate that possibility.

Conclusion

Our principal observations—a superexponential burst in the carbon cycle, the emergence of efficient acetoclastic methanogenesis, and a spike in the availability of nickel—appear straightforwardly related to several features of end-Permian environmental change: Siberian volcanism (7, 8), marine anoxia (5, 12, 13), and ocean acidification (14–16). A single horizontal gene transfer (17) instigated biogeochemical change, massive volcanism acted as a catalyst, and the resulting expansion of acetoclastic *Methanosarcina* acted to perturb CO_2 and O_2 levels. The ensuing biogeochemical disruption would likely have been widespread. For example, anaerobic methane oxidation may have increased sulfide levels (47), possibly resulting in a toxic release of hydrogen sulfide to the atmosphere, causing extinctions on land (48). Although such implications remain speculative, our work makes clear the exquisite sensitivity of the Earth system to the evolution of microbial life.

1. Erwin DH (2006) *Extinction: How Life on Earth Nearly Ended 250 Million Years Ago* (Princeton University Press, Princeton).
2. Shen SZ, et al. (2011) Calibrating the end-Permian mass extinction. *Science* 334(6061):1367–1372.
3. Holser WT, et al. (1989) A unique geochemical record at the Permian/Triassic boundary. *Nature* 337:39–44.
4. Magaritz M, Holser WT (1991) The Permian–Triassic of the Gartnerkofel-1 core (Carnic Alps, Austria): Carbon and oxygen isotope variation. *Abh Geol Bundesanst* 45:149–163.
5. Cao C, et al. (2009) Biogeochemical evidence for euxinic oceans and ecological disturbance presaging the end-Permian mass extinction event. *Earth Planet Sci Lett* 281(3-4):188–201.
6. Korte C, Kozur HW (2010) Carbon-isotope stratigraphy across the Permian–Triassic boundary: A review. *J Asian Earth Sci* 39(4):215–235.
7. Renne PR, Basu AR (1991) Rapid eruption of the Siberian Traps flood basalts at the Permo-Triassic boundary. *Science* 253(5016):176–179.
8. Reichow MK, et al. (2009) The timing and extent of the eruption of the Siberian Traps large igneous province: Implications for the end-Permian environmental crisis. *Earth Planet Sci Lett* 277(1-2):9–20.
9. Berner RA (2002) Examination of hypotheses for the Permo-Triassic boundary extinction by carbon cycle modeling. *Proc Natl Acad Sci USA* 99(7):4172–4177.
10. Ogden DE, Sleep NH (2012) Explosive eruption of coal and basalt and the end-Permian mass extinction. *Proc Natl Acad Sci USA* 109(1):59–62.
11. Svensen H, et al. (2009) Siberian gas venting and the end-Permian environmental crisis. *Earth Planet Sci Lett* 277(3-4):490–500.
12. Wignall PB, Twitchett RJ (1996) Oceanic anoxia and the end Permian mass extinction. *Science* 272(5265):1155–1158.
13. Isozaki Y (1997) Permo-Triassic boundary superanoxia and stratified superocean: Records from lost deep sea. *Science* 276(5310):235–238.
14. Knoll AH, Bambach RK, Canfield DE, Grotzinger JP (1996) Comparative Earth history and Late Permian mass extinction. *Science* 273(5274):452–457.
15. Knoll AH, Bambach RK, Payne JL, Pruss S, Fischer WW (2007) Paleophysiology and end-Permian mass extinction. *Earth Planet Sci Lett* 256(3-4):295–313.
16. Payne JL, Clapham ME (2012) End-Permian mass extinction in the oceans: An ancient analog for the twenty-first century? *Annu Rev Earth Planet Sci* 40:89–111.
17. Fournier GP, Gogarten JP (2008) Evolution of acetoclastic methanogenesis in *Methanosarcina* via horizontal gene transfer from cellulolytic *Clostridia*. *J Bacteriol* 190(3):1124–1127.
18. Diekert G, Konheiser U, Piechulla K, Thauer RK (1981) Nickel requirement and factor F430 content of methanogenic bacteria. *J Bacteriol* 148(2):459–464.
19. Konhauser KO, et al. (2009) Oceanic nickel depletion and a methanogen famine before the Great Oxidation Event. *Nature* 458(7239):750–753.
20. Rothman DH, Hayes JM, Summons RE (2003) Dynamics of the Neoproterozoic carbon cycle. *Proc Natl Acad Sci USA* 100(14):8124–8129.
21. Payne JL, et al. (2004) Large perturbations of the carbon cycle during recovery from the end-Permian extinction. *Science* 305(5683):506–509.
22. Rampino MR, Prokoph A, Adler A (2000) Tempo of the end-Permian event: High-resolution cyclostratigraphy at the Permian–Triassic boundary. *Geology* 28(7):643–646.
23. Archer D (2009) *The Long Thaw* (Princeton University Press, Princeton).
24. Pierrehumbert RT (2010) *Principles of Planetary Climate* (Cambridge University Press, Cambridge).
25. Hedges JI, Keil RG (1995) Sedimentary organic matter preservation: An assessment and speculative synthesis. *Mar Chem* 49(2-3):81–115.
26. Milkov A (2004) Global estimates of hydrate-bound gas in marine sediments: How much is really out there? *Earth Sci Rev* 66(3-4):183–197.
27. Ferry JG (1992) Methane from acetate. *J Bacteriol* 174(17):5489–5495.
28. Berger S, Welte C, Deppenmeier U (2012) Acetate activation in *Methanosaeta thermophila*: Characterization of the key enzymes pyrophosphatase and acetyl-CoA synthetase. *Archaea* 2012:315153.
29. Welte C, Deppenmeier U (2011) Membrane-bound electron transport in *Methanosaeta thermophila*. *J Bacteriol* 193(11):2868–2870.
30. Barber RD, et al. (2011) Complete genome sequence of *Methanosaeta concilii*, a specialist in aceticlastic methanogenesis. *J Bacteriol* 193(14):3668–3669.
31. Mori K, Iino T, Suzuki KI, Yamaguchi K, Kamagata Y (2012) Aceticlastic and NaCl-requiring methanogen "*Methanosaeta pelagica*" sp. nov., isolated from marine tidal flat sediment. *Appl Environ Microbiol* 78(9):3416–3423.
32. Min H, Zinder SH (1989) Kinetics of acetate utilization by two thermophilic acetotrophic methanogens: *Methanosarcina* sp. strain cals-1 and *Methanothrix* sp. strain cals-1. *Appl Environ Microbiol* 55(2):488–491.
33. Horita J, Zimmermann H, Holland HD (2002) Chemical evolution of seawater during the Phanerozoic: Implications from the record of marine evaporites. *Geochim Cosmochim Acta* 66(21):3733–3756.
34. Newton RJ, Pevitt EL, Wignall PB, Bottrell SH (2004) Large shifts in the isotopic composition of seawater sulphate across the Permo-Triassic boundary in northern Italy. *Earth Planet Sci Lett* 218(3-4):331–345.
35. Bottrell SH, Newton RJ (2006) Reconstruction of changes in global sulfur cycling from marine sulfate isotopes. *Earth Sci Rev* 75(1-4):59–83.
36. Luo G, et al. (2010) Isotopic evidence for an anomalously low oceanic sulfate concentration following end-Permian mass extinction. *Earth Planet Sci Lett* 300(1-2):101–111.
37. Blank CE (2009) Not so old Archaea - the antiquity of biogeochemical processes in the archaeal domain of life. *Geobiology* 7(5):495–514.
38. Fenchel T, Finlay BJ (1995) *Ecology and Evolution in Anoxic Worlds* (Oxford University Press, New York).
39. Schluter D (2000) *The Ecology of Adaptive Radiation* (Oxford University Press, New York).
40. Ragsdale SW (2009) Nickel-based enzyme systems. *J Biol Chem* 284(28):18571–18575.
41. Kaiho K, et al. (2001) End-Permian catastrophe by a bolide impact: Evidence of a gigantic release of sulfur from the mantle. *Geology* 29(9):815–818.
42. Naldrett AJ (2004) *Magmatic Sulfide Deposits: Geology, Geochemistry and Exploration* (Springer, New York).
43. Jacobs L, Emerson S, Huested SS (1987) Trace metal geochemistry in the Cariaco Trench. *Deep-Sea Res Part A* 34(5-6):965–981.
44. Haraldsson C, Westerlund S (1988) Trace metals in the water columns of the Black Sea and Framvaren Fjord. *Mar Chem* 23(3-4):417–424.
45. Lewis BL, Landing WM (1992) The investigation of dissolved and suspended-particulate trace metal fractionation in the Black Sea. *Mar Chem* 40:105–141.
46. Froelich PN, et al. (1979) Early oxidation of organic-matter in pelagic sediments of the eastern equatorial Atlantic: Suboxic diagenesis. *Geochim Cosmochim Acta* 43(7):1075–1090.
47. Kaiho K, et al. (2012) Changes in depth-transect redox conditions spanning the end-Permian mass extinction and their impact on the marine extinction: Evidence from biomarkers and sulfur isotopes. *Global Planet Change* 94-95:20–32.
48. Kump LR, Pavlov A, Arthur MA (2005) Massive release of hydrogen sulfide to the surface ocean and atmosphere during intervals of oceanic anoxia. *Geology* 33(5):397–400.

EARTH, ATMOSPHERIC, AND PLANETARY SCIENCES

EVOLUTION